ACS APPLIED MATERIALS & INTERFACES

Research Article

www.acsami.org

Carbon-Free CoO Mesoporous Nanowire Array Cathode for High-Performance Aprotic Li−O_2 Batteries

Baoshan Wu,[†] Hongzhang Zhang,*[,†] Wei Zhou,[†,‡] Meiri Wang,[†] Xianfeng Li,[†] and Huamin Zhang*[,†]

[†]Energy Storage Division, Dalian Institute of Chemical Physics, Chinese Academy of Sciences, Dalian 116023, P. R. China

[‡]University of Chinese Academy of Sciences, Beijing 100049, P. R. China

Supporting Information

ABSTRACT: Although various kinds of catalysts have been developed for aprotic Li−O_2 battery application, the carbon-based cathodes are still vulnerable to attacks from the discharge intermediates or products, as well as the accompanying electrolyte decomposition. To ameliorate this problem, the free-standing and carbon-free CoO nanowire array cathode was purposely designed for Li−O_2 batteries. The single CoO nanowire formed as a special mesoporous structure, owing even comparable specific surface area and pore volume to the typical Super-P carbon particles. In addition to the highly selective oxygen reduction/evolution reactions catalytic activity of CoO cathodes, both excellent discharge specific capacity and cycling efficiency of Li−O_2 batteries were obtained, with 4888 mAh g_{CoO}^{-1} and 50 cycles during 500 h period. Owing to the synergistic effect between elaborate porous structure and selective intermediate absorption on CoO crystal, a unique bimodal growth phenomenon of discharge products was occasionally observed, which further offers a novel mechanism to control the formation/decomposition morphology of discharge products in nanoscale. This research work is believed to shed light on the future development of high-performance aprotic Li−O_2 batteries.

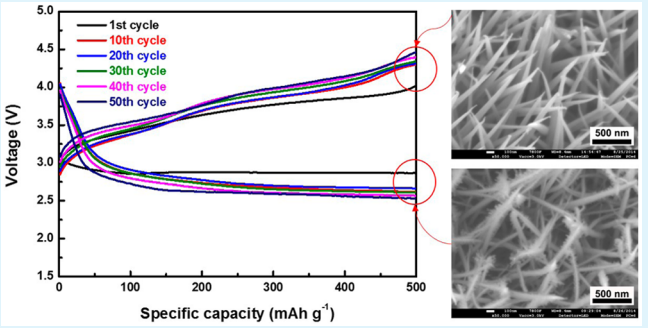

KEYWORDS: *Li−O_2 battery, CoO nanowire, carbon-free cathode, synergistic effect, Li−air*

1. INTRODUCTION

Li−O_2 battery is one of the most promising energy storage systems for its high theoretical specific energy density (>3500 Wh kg^{-1}) and potential application in electric transportation (>500 km range per single charge).[1−3] Among the four kinds of Li−O_2 batteries (aprotic, aqueous, solid-state, and hybrid aqueous/aprotic),[4] the aprotic ones possess higher theoretical gravimetric and volumetric capacities.[5] However, the relatively poor stability of aprotic electrolytes against discharge intermediates (LiO_2[6,7]) and products (Li_2O_2[8]) is really a big barrier before commercialization, for heavily decreasing the round trip efficiency and cycle life.[9,10] During the recent years, many efforts have been engaged in solving this problem, such as developing novel solvents (e.g., TEGDME,[8,11] DMSO[12,13]), developing novel electrolyte additives,[14−16] and so on. As a common consideration, the cathode material plays a key role in the electrolyte stabilization, owing to the synergistic effect between cathode materials and aprotic electrolytes involved in the three-phase boundary (cathode materials, liquid electrolyte, and O_2).[17,18] Besides that, the columbic efficiency and voltage polarization during cycling are also heavily affected by the cathode material, rendering it as the key component for Li−O_2 battery development.[19]

The ideal cathode material of Li−O_2 battery should be capable of transporting electrons and reactants (Li-ion and O_2), depositing discharge products,[11,20,21] and affording high activity for the interfacial oxygen reduction/evolution reactions (ORR/OER) and low activity for the harmful parasitic reactions.[12,22] Among plenty of materials, carbon is usually chosen to construct the cathodes, due to the advantages of low cost, high electrical conductivity, diverse structure, and functional surface.[11,21,23−28] However, the carbon/electrolyte interface is unstable during the charge/discharge process.[29] Although some kinds of catalysts loaded on carbon cathodes could help to relieve this issue,[15,30−35] carbon materials cannot be permanently stable with discharge intermediates and products.[36−39] Even the ordinary polymer binders are suggested to be abandoned, to avoid harmful oxidative degradation during the cycling process.[38,39] Thus, some kinds of pure metals (e.g., Au[12,40] and Pd[41]) and metal oxides (e.g., Co_3O_4,[42−45] MnO_2,[46] TiO_2,[47] and $(Co,Mn)_3O_4$[48]) have been developed as a novel generation of Li−O_2 cathode materials, significantly improving the battery stability.

Among most noncarbon materials, cobalt monoxide (CoO) has attracted great attention for electrochemical energy devices (Li-ion batteries,[49,50] supercapacitors,[51,52] fuel cells,[53−55] etc.) due to the satisfying electrochemical activities. By adding a portion of mesoporous CoO nanoparticles, $CoSe_2$/CoO nanocomposites, CoO mesoporous spheres, or oxygen vacancy-

Received: July 31, 2015
Accepted: September 24, 2015
Published: September 24, 2015

DOI: 10.1021/acsami.5b07003
ACS Appl. Mater. Interfaces 2015, 7, 23182−23189

bearing CoO nanoparticles into the carbon-based cathode, the cycle stability of Li−O_2 battery has been improved to some extent.[56−59] As for the pure CoO carbon-free cathode, however, the ORR/OER activity and structure−performance-relationship in aprotic Li−O_2 batteries have not been reported yet. In addition, how to construct CoO framework with considerable surface area and properly porous structure was also deemed as a great challenge in this area.

On the basis of the above consideration, a carbon-free cathode built with free-standing CoO nanowire arrays on Ni-foam was primarily designed for aprotic Li−O_2 batteries in our lab. This cathode could offer enormous free volume among the nanowire arrays and inside each single nanowire, even achieving a similar specific surface area to that of carbon materials such as Super-P. Benefiting from the unique nanoscale architecture, carbon-free material and high catalytic interface, the as-designed Li−O_2 cathode should possess excellent capability to accommodate the discharge products as well as to confine the side reactions during battery cycling process. As a result, the Li−O_2 batteries showed high specific capacity (4888 mAh g_{CoO}^{-1}) and long-term cycle life (50 cycles, 500 h), which was among the highest value for the carbon-free materials. In the following article, the structure control of the carbon-free CoO nanowire array cathode was illustrated in detail, with the structure−performance relationship in aprotic Li−O_2 batteries thoroughly discussed.

2. EXPERIMENTAL SECTION

2.1. Cathode Preparation. The mesoporous CoO nanowire array cathodes were prepared via hydrothermal process followed with calcination,[49,51] as illustrated in Scheme 1. In detail, a Ni-foam substrate (LIRUN, MF003) was first smoothed through cold-press and punched into 2 cm^2 disks. After they were ultrasonically cleaned successively in 6 M HCl, deionized water, and acetone for 30 min, the disks were weighed and vertically assembled into glass tubes. Second, 0.582 g (2 mmol) of $Co(NO_3)_2{\cdot}6H_2O$ and 0.6 g (10 mmol) of $CO(NH_2)_2$ were dissolved into 50 mL of deionized water under stirring for 30 min at room temperature. Third, the as-prepared homogeneous solution was transferred into a 100 mL Teflon-lined stainless steel autoclave containing six clean Ni-foam disks in two glass tubes vertically aligned with the bottom. After the precursors were grown on Ni-foam through 8 h of hydrothermal process at 95 °C, the disks were washed thoroughly with deionized water and ethanol and then were calcinated at 450 °C for 4 h under a constant flow of Ar_2. The samples with the CoO loading amount of 0.7−0.9 mg cm^{-2} were selected as cathodes for further research. For comparison, carbon cathodes made from commercial carbon blacks (Super-P from TIMCAL) as active material and polytetrafluoroethylene (PTFE) as polymer binder were prepared on Ni-foam disks through drop-casting and heat treatment. Briefly, 10 mg of Super-P powder and 50 mg of PTFE suspension (dispersion in water, 5 wt % solids) were ultrasonically dispersed in 10 mL isopropanol for 1 h at room temperature. The Super-P/PTFE suspension was then drop-cast onto the weighed Ni-foam disks and dried at 120 °C air-dry oven for several times, until the Super-P loading amount of each disk was up to 0.8 mg cm^{-2}.

Scheme 1. Schematic Illustration for Preparation of CoO Nanowire Arrays on Ni-Foam

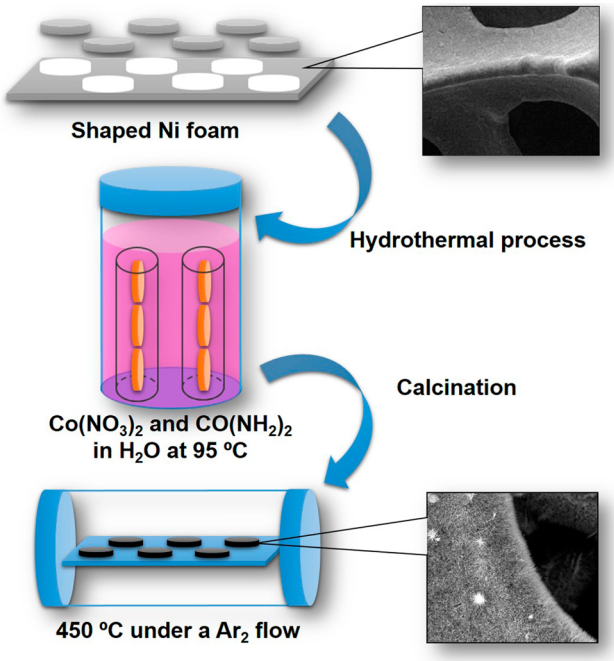

2.2. Material Characterization. The crystal phase of samples was characterized via X-ray powder diffraction equipment (PANalytical, monochromatic Cu Kα radiation 30 mA, 40 kV). N_2 adsorption isotherms were measured at 77.3 K using an ASAP2010 system (Micromeritics, USA). Surface areas and pore volumes were determined using Brunauer−Emmett−Teller (BET) method. The pore size distribution curves were calculated from the desorption branches of nitrogen isotherms according to the Barrett−Joyner−Halenda (BJH) model. The material morphology and microstructure were observed with scanning electronic microscope (SEM, QUANTA-200F at an acceleration voltage of 20 kV or JSM-7800F at an acceleration voltage of 3 kV) and transmission electron microscopy (TEM, Tecnai G2 F20).

2.3. Electrochemical Activity Measurement. Cyclic voltammetry (CV) measurement was applied to study the ORR/OER catalytic activity of the prepared materials with a three-electrode system. The working electrode was prepared by loading the sample of 0.02 mg cm^{-2} on glassy carbon electrode. First, 1 mg of sample (CoO nanowire powder or Super-P powder) and 15 μL of 5 wt % Nafion solution (EW = 1000, DuPont) were dispersed in 0.5 mL of isopropanol by 30 min of sonication at room temperature. The as-prepared suspension (5 μL) and 5 μL of 5 wt % Nafion solution were orderly cast on the glassy carbon working electrode of 4 mm in diameter (loading 0.02 mg cm^{-2}). CVs were conducted with a potentiostat (Pine) in a three-electrode electrochemical cell using lithium-foils as both counter electrode and reference electrode. Electrolyte was 1.0 M bis (trifluoromethane) sulfonamide lithium (LiTFSI) dissolved in tetraethylene glycol dimethylether (TEGDME), which was bubbled with O_2 for 1 h before measurements. CV curves were scanned at a rate of 10 mV s^{-1} between 4.3 and 2 V with a constant O_2 bubbling during measurement.

2.4. Li−O_2 Battery Performance Test. Li−O_2 batteries were assembled with cathodes made of above-mentioned CoO nanowire arrays or Super-P/PTFE composites on Ni-foam disks, 0.45 mm thick Li disks (16 mm in diameter) as anodes, and polypropylene fibers (Novatexx 2471 Freudenberg Filtration Technologies KG) saturated with electrolyte (1.0 M LiTFSI in TEGDME) as separators in homemade cell model. The charge/discharge performance of the Li−O_2 battery was tested with LAND 2100 system (Wuhan, China) under the constant current mode. The charge/discharge profiles were measured at a current density of 20 mA g^{-1} (with cutoff voltages of 2 V in discharge and 4.3 V in charge) and 100 mA g^{-1} (with cutoff specific capacity of 500 mAh g^{-1} for charge/discharge). The current density was calculated based on the mass of CoO or Super-P loading.

3. RESULTS AND DISCUSSION

3.1. Cathode Composition and Structure. Figure 1a presents X-ray diffraction (XRD) patterns of as-synthesized CoO, Ni-foam, and the reported ones. The pattern of CoO matches well with the reported one (JCPDS Card No. 01−071−4749) as well as the published results in which the sample is single-crystalline in nature.[49] In addition, all visible peaks of CoO grown on the Ni foam can be readily assigned to the cubic CoO

DOI: 10.1021/acsami.5b07003
ACS Appl. Mater. Interfaces 2015, 7, 23182−23189

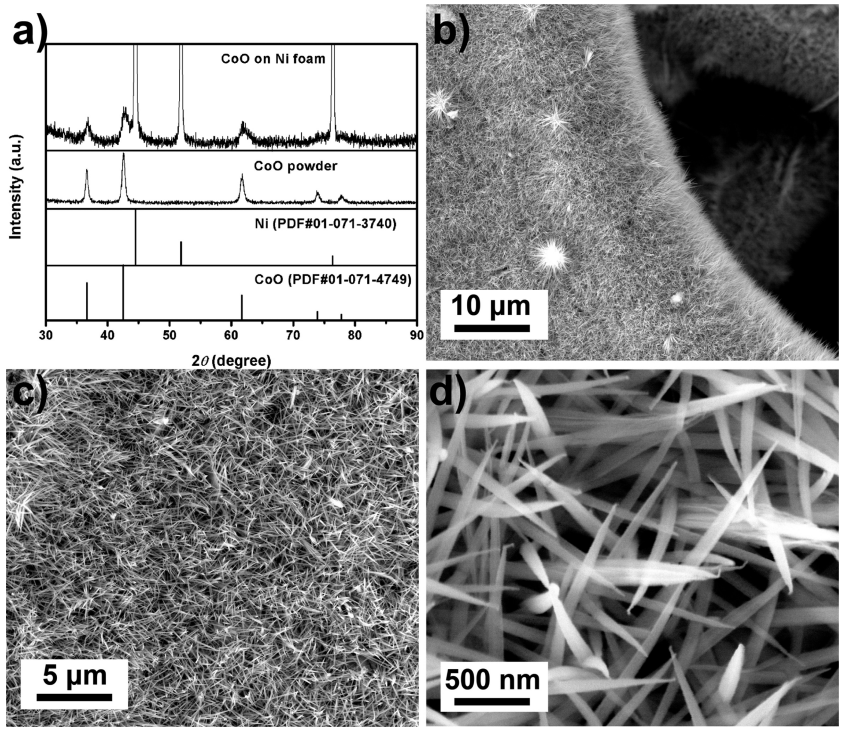

Figure 1. (a) Experimental and reported XRD patterns of CoO and Ni. FESEM images of CoO nanowires grown on Ni-foam in (b) low magnification, (c) middle magnification, and (d) high magnification via QUANTA-200F at an acceleration voltage of 20 kV.

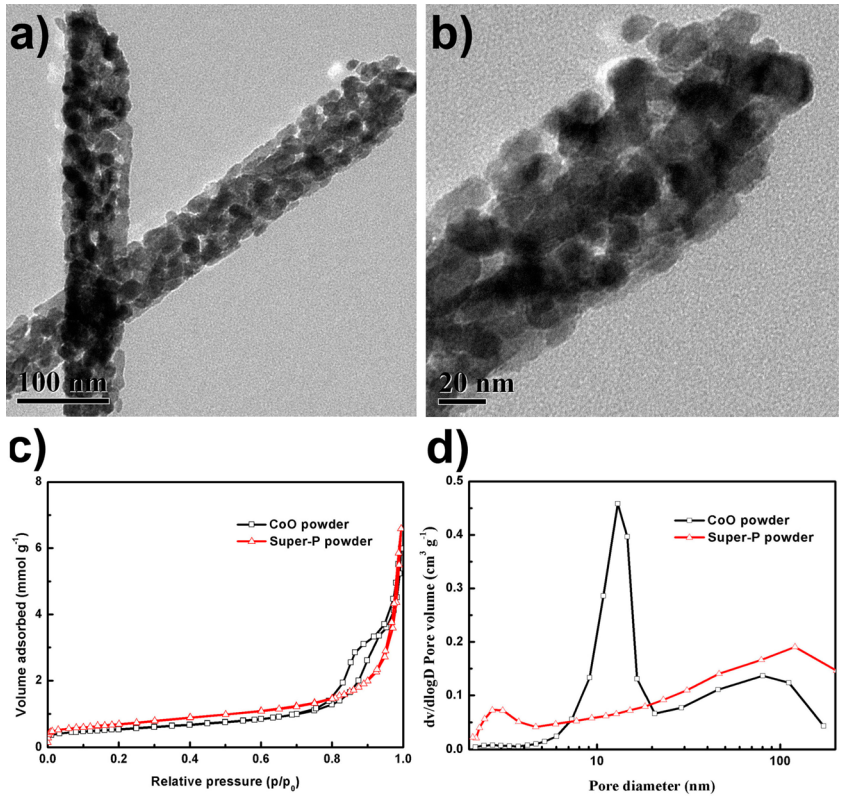

Figure 2. TEM images of CoO nanowires in (a) low magnification and (b) high magnification. (c) Nitrogen adsorption/desorption isotherms and (d) pore size distribution of CoO powder and Super-P powder.

and Ni (JCPDS Card No. 01−071−3740), which indicates no impurity exists.

The morphology of the obtained CoO nanowire arrays on Ni-foam was investigated via field-emission scanning electron microscopy (FESEM). According to the side view of CoO nanowires in Figure 1b, the length of CoO nanowires is typically 3−5 μm. As shown in Figure 1c, it is obvious that the three-dimensional arrays assembled with CoO nanowires are directly

DOI: 10.1021/acsami.5b07003
ACS Appl. Mater. Interfaces 2015, 7, 23182−23189

and uniformly grown on the Ni-foam substrate, which is in favor of enhancing electrical conductivity and mechanical strength at the joints.[45] Also, a magnified FESEM image in Figure 1d indicates that the nanowires have sharp tips and good uniformity with diameter of ca. 80 nm. The L/D (length/diameter) ratio of this structure is nearly 50:1, forming a highly porous network with the pore diameter of 30−300 nm, which is benefit to accommodating the discharge products as well as transporting Li-ion and O_2.

The internal structure of CoO nanowires was further characterized by transmission electron microscopy (TEM). As shown in Figure 2a,b, every CoO nanowire contains numerous interconnected nanoparticles (ca. 20 nm in diameter), which further provides large quantity of mesopores for the deposition of discharge products. The specific surface and porous property of the CoO nanowires and Super-P particles were investigated with BET method. As shown in Figure 2c, the nitrogen adsorption and desorption isotherms indicate that both CoO and Super-P possess a typical isotherm with a hysteresis loop, which is in accordance with a highly mesoporous structure. In contrast with Super-P powder, CoO powder possesses similar surface area (42 $m^2\ g^{-1}$), approximate pore volume (0.21 $cm^3\ g^{-1}$), and more pores in small size (<15 nm, 42%) in Table 1, which is advantageous to confine the growth of discharge products.

Table 1. Porosity parameters of CoO and Super-P powders

material	S_{BET} [$m^2\ g^{-1}$]	V_{total} [$cm^3\ g^{-1}$]	$V_{<15\ nm}$ [$cm^3\ g^{-1}$]	$V_{15-300\ nm}$ [$cm^3\ g^{-1}$]
Super-P	54	0.228	0.042 (18%)	0.186 (82%)
CoO	42	0.208	0.088 (42%)	0.120 (58%)

To further explore the structural differences between as-synthesized CoO and Super-P cathodes, the morphology of Super-P cathodes was also investigated with FESEM as shown in Figure S1. Compared with the disorder structure of Super-P cathodes, the array structure of CoO cathodes shows many more advantages. For one thing, the single nanowire is an internal high-quality crystal, which assures quick electron transport compared to that of the loosely binding carbon powders.[60] For another thing, the nanowires are directly grown on the current collector, which could further reduce the contact resistance. In addition, the nanowires are mutually separated and possess high aspect-ratio, which means that there exists much larger surface area directly exposed to the external environment than disorder piling nanoparticles. And large quantities of mesopores within nanowires could provide plenty of channels for Li-ion and O_2 penetration into the inner region. So, both external and internal surface of CoO nanowires are of high usability for ORR/OER, while the nanoscale pores of Super-P cathode are always blocked by numerous unwanted interfaces as shown in Figure S1.[61] Beyond high utilization of active surface, the well-separated nanowires form a large amount of open macropores, which could be efficiently used as channels to transport Li-ion and O_2. Besides that, the CoO nanowire cathodes avoid the use of polymer binders and conductive additives, which substantially reduces the useless surface in oxygen electrode. Also, the calcinated nanowire array is mechanically robust not only inside the nanowires but also between nanowires and current collectors, which can greatly reduce the potential structure damage caused by product deposition during discharge process. To put it in a nutshell, the CoO nanowire array structure takes advantages of good electron transport, high utilization of surface, high-efficient channels, and robust mechanical property to improve the energy output and cycle life in Li−O_2 batteries.

3.2. ORR/OER Activity and Stability. To further determine the universal catalytic activity of as-synthesized CoO nanowires without the influence of variables induced by full cell assembly testing, the ORR/OER activity and stability were evaluated in O_2-saturated 1.0 M LiTFSI in TEGDME, as shown in Figure 3.

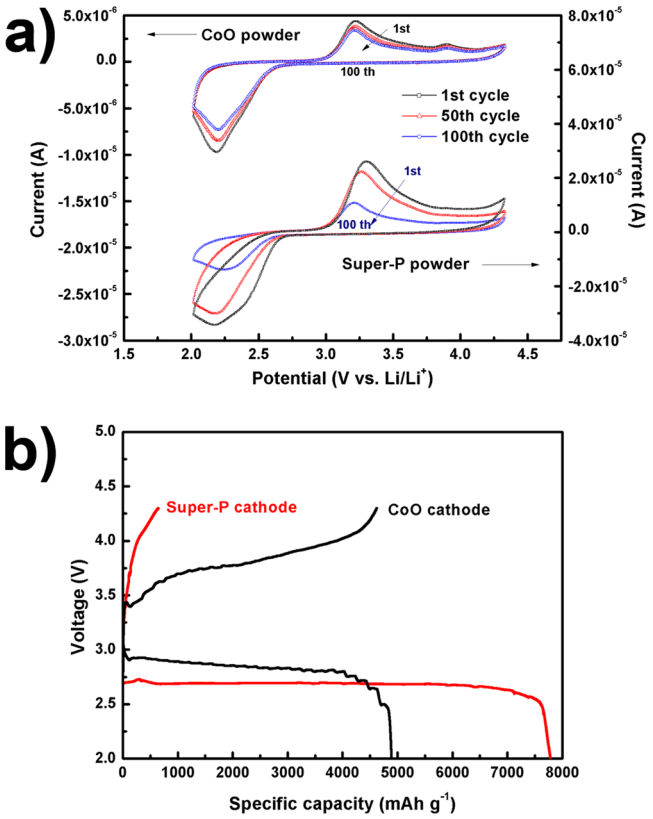

Figure 3. (a) CV curves of cycles 1, 50, and 100 of CoO powder and Super-P powder on glassy carbon electrodes in O_2-saturated 1.0 M LiTFSI/TEGDME solution. (b) Discharge−charge profiles of the CoO and Super P cathodes measured at 20 mA g^{-1} with 2 V discharge and 4.3 V charge cutoff voltages in Li−O_2 battery tests (the specific capacity is calculated with respect to the mass of CoO or Super-P).

Figure 3a presents CV curves of cycles 1, 50, and 100 for CoO powder and Super-P powder on glassy carbon electrodes. Although CoO nanowires and Super-P nanoparticles could activate ORR/OER in aprotic electrolyte, the peak currents of Super-P nanoparticles are obviously higher than the ones of CoO nanowires, which should be related to the larger active specific area and better electrical conductivity of Super-P nanoparticles than the CoO nanowires in form of the randomly packed network. For the ORR/OER activity of Super-P nanoparticles, the peak currents gradually decrease during cycling, which may be induced by the decomposition residues of electrolyte covered on reactive sites.[19] It is noted that CoO nanowires exhibit more stable peak current and potential during 100 cycles, which should be related to the preferential absorption of discharge intermediates on CoO rather than carbon materials to further protect electrolyte from the attack of discharge intermediates.[57,58] Besides the broad peak at 3.2 V corresponding to decomposition of Li_2O_2, there is a small peak at 3.9 V during oxidation process for CoO nanowires, which was also observed on Ru electrodes and can be attributed to the decomposition of

DOI: 10.1021/acsami.5b07003
ACS Appl. Mater. Interfaces 2015, 7, 23182−23189

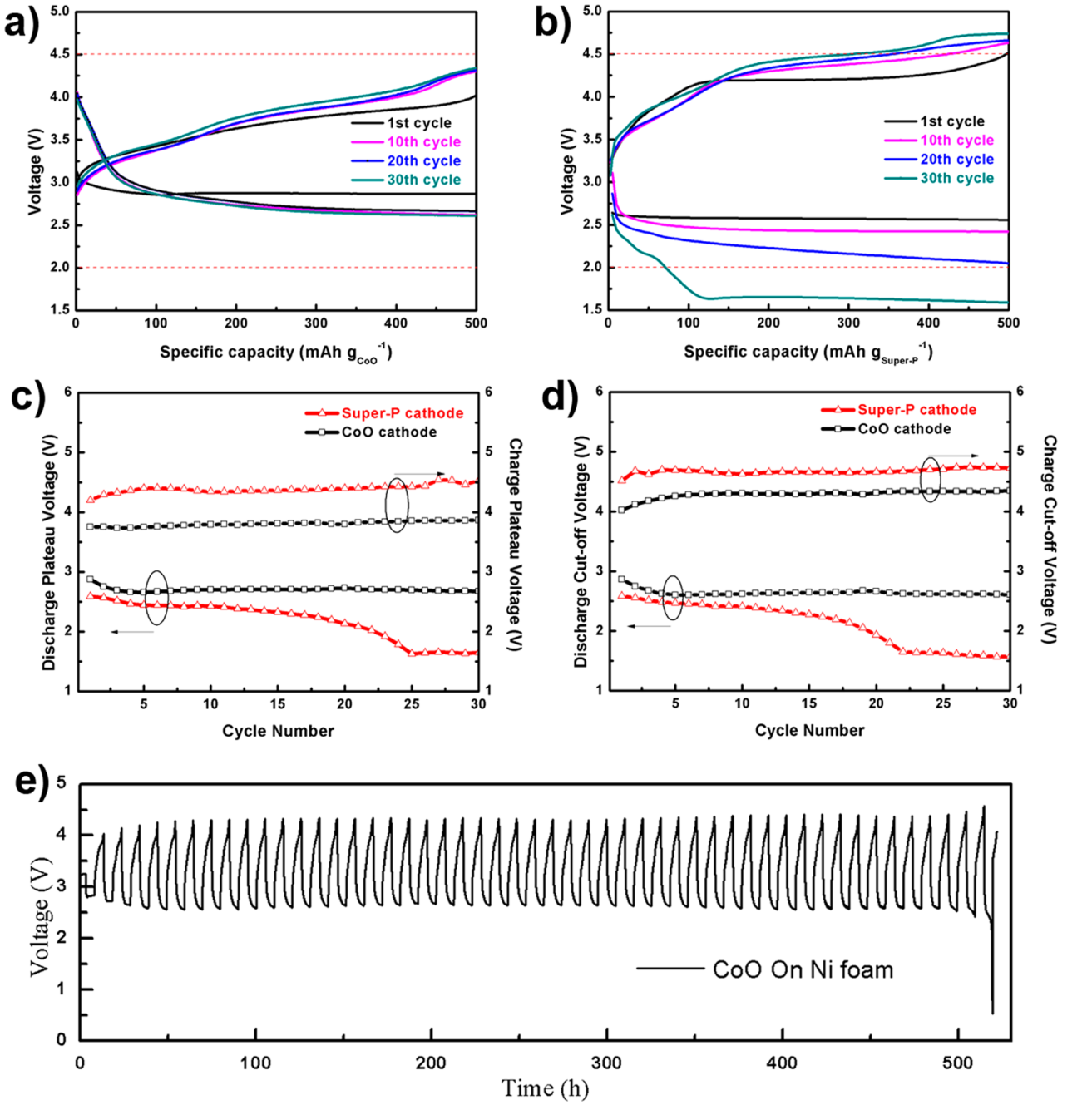

Figure 4. Discharge−charge profiles of cycles 1, 10, 20, and 30 with (a) CoO cathodes and (b) Super-P cathodes as oxygen electrodes measured at 100 mA g^{-1} with 500 mAh g^{-1} cutoff specific capacity (the specific capacity is calculated with respect to the mass of CoO or Super-P). (c) Discharge−charge plateau voltages and (d) discharge−charge cutoff voltages of CoO cathode and Super-P cathode vs cycle number during 30 cycles (the plateau and cutoff voltages respectively correspond with the values at 250 and 500 mAh g^{-1}). (e) Cycle performance of the CoO cathodes measured at 100 mA g^{-1} with 500 mAh g^{-1} cutoff specific capacity based on the mass of CoO during more than 500 h of discharge−charge time.

side products rather than electrolyte decomposition as described by previous report.[62] For Super-P nanoparticles, there is no obvious peak at 3.9 V during oxidation process, which is consistent with previous research on glassy carbon electrodes and demonstrates that side products were not decomposed during oxidation process.[7,18,62] As a result, the enhanced ORR/OER stability could lead to improvements in the rechargeable characterization and the round-trip efficiency of aprotic Li−O_2 batteries.

The charge/discharge performance of Li−O_2 batteries assembled with CoO and Super-P cathodes was also investigated by cycling at 20 mA g^{-1} with cutoff voltages at 4.3 and 2 V. According to the voltage−capacity profiles in Figure 3b, the specific discharge capacities of CoO nanowires and Super-P nanoparticles are, respectively, 4888 mAh g_{CoO}^{-1} and 7783 mAh g_{carbon}^{-1}. Although the specific discharge capacity of CoO cathodes is only 60% of that of Super-P cathodes, it is still higher than the reported values of Co_3O_4 nanowire cathodes at the roughly same current density.[43,45] Note that more than 80% discharge−charge progresses of CoO cathodes showed potential gap below 1.25 V, especially below 1 V at the half of discharge

DOI: 10.1021/acsami.5b07003
ACS Appl. Mater. Interfaces 2015, 7, 23182−23189

capacity, showing obviously improved ORR/OER activity compared to that of Super-P cathodes.

In addition, the superior ORR/OER activity of CoO cathodes was more obvious in cycling tests, during which both cathodes were measured at 100 mA g^{-1} with 500 mAh g^{-1} cutoff specific capacity. As shown in Figure 4a,b, the cycle stability of the CoO cathodes is significantly better than that of Super-P cathodes during the initial 30 cycles. According to Figure 4c, the middle discharge and charge plateau voltages of CoO cathodes were above 2.6 and below 3.9 V, respectively, while that of the Super-P cathodes reached 2.0 and 4.6 V, respectively, at the end of the 30th cycle. Figure 4d further presents the variation of cutoff voltages during the 30 cycles, in which the CoO cathodes also show higher discharge voltage (>2.6 V) and lower charge voltage (<4.4 V) than the Super-P cathodes.

Besides that, the batteries assembled with CoO cathodes were cycled 50 times (>500 h) at 100 mA g^{-1} with 500 mAh g^{-1} cutoff specific capacity. As shown in Figure 4e, the discharge and charge voltages are, respectively, above 2.5 and below 4.5 V, which are comparable with the previous reports of Co_3O_4 nanowire cathodes at the same current density and cycling duration.[43] At the end of the cycling test, the lithium anodes have been transformed into the white powders instead of the original shiny disks, which indicates that the malfunction was mainly caused by the complete consumption of lithium foil as reported elsewhere.[63] In short, the excellent capacity and cycling performance are ascribed to the mesoporous nanowire array architecture and stable surface activity of CoO cathodes, in which the architecture can fast transport the reactants to the stable and efficient surface and largely store discharge products in mesopores to improve ORR process, and vice versa for OER process.

3.3. Cathode Morphology during Cycling. To further investigate the mechanism of deposition/decomposition of solid discharge products, the morphology of CoO cathodes was characterized by FESEM after the initial first discharge and first charge at 100 mA g^{-1} with 500 mAh g^{-1} cutoff specific capacity. As shown in Figure 5 and Figure S3, it is obvious that the growth

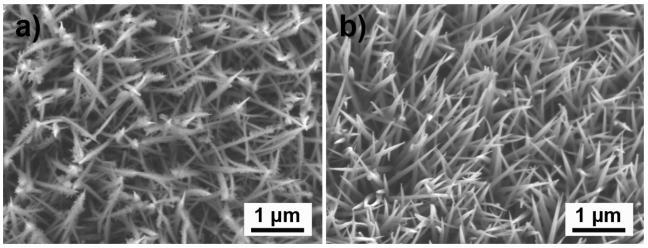

Figure 5. FESEM images of CoO cathode via JSM-7800F at an acceleration voltage of 3 kV after the initial 1st discharge (a) and 1st charge (b) at 100 mA g^{-1} with 500 mAh g^{-1} cutoff specific capacity.

of discharge products on CoO cathodes follows the branch-like type rather than the membrane-like type on Super-P cathodes in Figure S2. As for the branch-like type growth, plenty of active sites could be permanently exposed to the three-phase boundary rather than covered by discharge products for membrane-like type. And at the end of the first charge process, the smooth surface of CoO nanowires (Figure 5b) indicates that the discharge products were effectively decomposed during charge process. It is important to point out that the decomposition of Li_2O_2 and side products can, respectively, process at 3.2 and 3.9 V in Figure 3a, and the potential is less than 3.9 V during the most first charge process for CoO cathode in Figure 4a, which means that the major discharge product should be Li_2O_2 rather than side products.[43] As for the membrane-like type growth, however, the discharge products on Super-P cathodes are continuously connected with each other on adjacent carbon particles in accord with the previous reports.[11,64,65] As a result, the electrochemical active sites for ORR/OER on Super-P cathodes are separated from reactants, with the transport channels of Li-ion and O_2 being blocked, finally leading to the high overpotential gaps (Figure 4b). It is noteworthy that the branch-like growth type on CoO cathodes has not been reported in previous studies of the column-like discharge morphology on Co_3O_4 cathodes.[43,45] Although the reliable reason why the discharge products are grown on CoO nanowires along the specific orientation is still unclear, it should be related to the different binding properties for LiO_2 adsorption on various crystal planes, such as Co−CoO (111), CoO (110), CoO (100), CoO (200), CoO (220), and O−CoO (111), on the basis of previous DFT calculations.[57] Also, the correlation between index facet of crystal planes and density of reactive sites was revealed for gold nanocrystals applied in Li−O_2 batteries in previous research.[66] Besides the branch-like type growth on the surface of CoO nanowires, the growth of discharge products could be further confined by mesopores inside the CoO nanowires as shown in Figure 2b and previous studies.[28,31,44] The simultaneous outside branch-like growth and inside particle-like growth are named as bimodal growth, with the size of discharge products differing obviously in nanoscale. Compared with microscale discharge products in Super-P cathodes, the nanoscale products of bimodal growth have a higher surface area-to-volume ratio, which could further benefit the surface delithiation and accelerate the electrochemical decomposition process.[67−69] On the basis of this consideration, the excellent cycling stability of CoO cathodes could be well-explained.

4. CONCLUSION

To summarize, the carbon-free cathode based on pure CoO mesoporous nanowire arrays was first proposed and systematically studied for aprotic Li−O_2 battery application. It achieved a specific capacity over 4800 mAh g_{CoO}^{-1} and long-term stability of 50 cycles during 500 h, ascribed to the unique porous architecture and high ORR/OER catalytic activity on the CoO surface. Furthermore, the specific bimodal growth of discharge products occurred on both the interior and exterior surfaces of the CoO nanowire, due to the synergistic effect between selective absorption and geometric confinement on the CoO crystal faces and inside the mesoporous structure. All in all, this research put forward the morphology control mechanism of discharge products and expanded the development of carbon-free cathodes, which is believed to be of great help in the future development of Li−O_2 batteries.

■ ASSOCIATED CONTENT

Supporting Information

The Supporting Information is available free of charge on the ACS Publications website at DOI: 10.1021/acsami.5b07003.

FESEM images of Super-P cathodes under different magnification. FESEM images of Super-P cathode in high-magnification and low-magnification after the initial 500 $mAhg^{-1}$ discharge at 100 mA g^{-1}. High-magnification FESEM images of CoO cathode after the initial 1st discharge at 100 mA g^{-1} with 500 mAh g^{-1} cutoff specific capacity. (PDF)

DOI: 10.1021/acsami.5b07003
ACS Appl. Mater. Interfaces 2015, 7, 23182−23189

AUTHOR INFORMATION

Corresponding Authors

*Phone: +86 411 8437 9669. Fax: +86 411 8466 5057. E-mail: zhanghz@dicp.ac.cn. (Hongzhang Zhang)

*Phone: +86 411 8437 9072. Fax: +86 411 8466 5057. E-mail: zhanghm@dicp.ac.cn. (Huamin Zhang)

Notes

The authors declare no competing financial interest.

ACKNOWLEDGMENTS

The authors acknowledge financial support from National Natural Science Foundation of China (Nos. 51403209, 21406221, and 51177156/E0712), Youth Innovation Promotion Association (CAS2015148), 100 Talents Program of Dalian Institute of Chemical Physics, Natural Sciences Foundation of Liaoning Province of China (2013020126), Hubei Province-Chinese Academy of Sciences Cooperative Project.

REFERENCES

(1) Abraham, K. M.; Jiang, Z. A Polymer Electrolyte-Based Rechargeable Lithium/Oxygen Battery. *J. Electrochem. Soc.* **1996**, *143*, 1−5.

(2) Girishkumar, G.; McCloskey, B.; Luntz, A. C.; Swanson, S.; Wilcke, W. Lithium-Air Battery: Promise and Challenges. *J. Phys. Chem. Lett.* **2010**, *1*, 2193−2203.

(3) Bruce, P. G.; Freunberger, S. A.; Hardwick, L. J.; Tarascon, J. M. Li-O2 and Li-S Batteries with High Energy Storage. *Nat. Mater.* **2012**, *11*, 172−172.

(4) Lu, J.; Li, L.; Park, J. B.; Sun, Y. K.; Wu, F.; Amine, K. Aprotic and Aqueous Li-O2 Batteries. *Chem. Rev.* **2014**, *114*, 5611−5640.

(5) Zheng, J. P.; Liang, R. Y.; Hendrickson, M.; Plichta, E. J. Theoretical Energy Density of Li-Air Batteries. *J. Electrochem. Soc.* **2008**, *155*, A432−A437.

(6) Peng, Z.; Freunberger, S. A.; Hardwick, L. J.; Chen, Y.; Giordani, V.; Bardé, F.; Novák, P.; Graham, D.; Tarascon, J. M.; Bruce, P. G. Oxygen Reactions in a Non-Aqueous Li+ Electrolyte. *Angew. Chem., Int. Ed.* **2011**, *50*, 6351−6355.

(7) Cao, R.; Walter, E. D.; Xu, W.; Nasybulin, E. N.; Bhattacharya, P.; Bowden, M. E.; Engelhard, M. H.; Zhang, J. G. The Mechanisms of Oxygen Reduction and Evolution Reactions in Nonaqueous Lithium-Oxygen Batteries. *ChemSusChem* **2014**, *7*, 2436−2440.

(8) Black, R.; Oh, S. H.; Lee, J. H.; Yim, T.; Adams, B.; Nazar, L. F. Screening for Superoxide Reactivity in Li-O2 Batteries: Effect on Li2O2/LiOH Crystallization. *J. Am. Chem. Soc.* **2012**, *134*, 2902−2905.

(9) Freunberger, S. A.; Chen, Y.; Drewett, N. E.; Hardwick, L. J.; Bardé, F.; Bruce, P. G. The Lithium-Oxygen Battery with Ether-Based Electrolytes. *Angew. Chem., Int. Ed.* **2011**, *50*, 8609−8613.

(10) Balaish, M.; Kraytsberg, A.; Ein-Eli, Y. A Critical Review on Lithium-Air Battery Electrolytes. *Phys. Chem. Chem. Phys.* **2014**, *16*, 2801−2822.

(11) Jung, H. G.; Hassoun, J.; Park, J. B.; Sun, Y. K.; Scrosati, B. An Improved High-Performance Lithium-Air battery. *Nat. Chem.* **2012**, *4*, 579−585.

(12) Peng, Z.; Freunberger, S. A.; Chen, Y.; Bruce, P. G. A Reversible and Higher-Rate Li-O2 Battery. *Science* **2012**, *337*, 563−566.

(13) Ottakam Thotiyl, M. M.; Freunberger, S. A.; Peng, Z.; Chen, Y.; Liu, Z.; Bruce, P. G. A Stable Cathode for the Aprotic Li-O2 Battery. *Nat. Mater.* **2013**, *12*, 1050−1056.

(14) Chen, Y.; Freunberger, S. A.; Peng, Z.; Fontaine, O.; Bruce, P. G. Charging a Li-O2 Battery Using a Redox Mediator. *Nat. Chem.* **2013**, *5*, 489−494.

(15) Lim, H. D.; Song, H.; Kim, J.; Gwon, H.; Bae, Y.; Park, K. Y.; Hong, J.; Kim, H.; Kim, T.; Kim, Y. H.; Lepró, X.; Ovalle-Robles, R.; Baughman, R. H.; Kang, K. Superior Rechargeability and Efficiency of Lithium-Oxygen Batteries: Hierarchical Air Electrode Architecture Combined with a Soluble Catalyst. *Angew. Chem., Int. Ed.* **2014**, *53*, 3926−3931.

(16) Sun, D.; Shen, Y.; Zhang, W.; Yu, L.; Yi, Z.; Yin, W.; Wang, D.; Huang, Y.; Wang, J.; Wang, D.; Goodenough, J. B. A Solution-Phase Bifunctional Catalyst for Lithium-Oxygen Batteries. *J. Am. Chem. Soc.* **2014**, *136*, 8941−8946.

(17) Lee, J. S.; Tai Kim, S.; Cao, R.; Choi, N. S.; Liu, M.; Lee, K. T.; Cho, J. Metal-Air Batteries with High Energy Density: Li-Air versus Zn-Air. *Adv. Energy Mater.* **2011**, *1*, 34−50.

(18) Gittleson, F. S.; Sekol, R. C.; Doubek, G.; Linardi, M.; Taylor, A. D. Catalyst and Electrolyte Synergy in Li-O2 Batteries. *Phys. Chem. Chem. Phys.* **2014**, *16*, 3230−3237.

(19) Li, F.; Tang, D. M.; Chen, Y.; Golberg, D.; Kitaura, H.; Zhang, T.; Yamada, A.; Zhou, H. Ru/ITO: A Carbon-Free Cathode for Nonaqueous Li-O2 Battery. *Nano Lett.* **2013**, *13*, 4702−4707.

(20) Xiao, J.; Wang, D.; Xu, W.; Wang, D.; Williford, R. E.; Liu, J.; Zhang, J. G. Optimization of Air Electrode for Li/Air Batteries. *J. Electrochem. Soc.* **2010**, *157*, A487−A492.

(21) Xiao, J.; Mei, D.; Li, X.; Xu, W.; Wang, D.; Graff, G. L.; Bennett, W. D.; Nie, Z.; Saraf, L. V.; Aksay, I. A.; Liu, J.; Zhang, J. G. Hierarchically Porous Graphene as a Lithium-Air Battery Electrode. *Nano Lett.* **2011**, *11*, 5071−5078.

(22) Zhang, T.; Zhou, H. A Reversible Long-Life Lithium-Air Battery in Ambient Air. *Nat. Commun.* **2013**, *4*, 1817.

(23) Li, Q.; Cao, R.; Cho, J.; Wu, G. Nanostructured Carbon-Based Cathode Catalysts for Nonaqueous Lithium-Oxygen Batteries. *Phys. Chem. Chem. Phys.* **2014**, *16*, 13568−13582.

(24) Wang, Z. L.; Xu, D.; Wang, H. G.; Wu, Z.; Zhang, X. B. In Situ Fabrication of Porous Graphene Electrodes for High-Performance Energy Storage. *ACS Nano* **2013**, *7*, 2422−2430.

(25) Guo, Z.; Zhou, D.; Dong, X.; Qiu, Z.; Wang, Y.; Xia, Y. Ordered Hierarchical Mesoporous/Macroporous Carbon: A High-Performance Catalyst for Rechargeable Li-O2 Batteries. *Adv. Mater.* **2013**, *25*, 5668−5672.

(26) Chen, Y.; Li, F.; Tang, D. M.; Jian, Z.; Liu, C.; Golberg, D.; Yamada, A.; Zhou, H. Multi-Walled Carbon Nanotube Papers as Binder-Free Cathodes for Large Capacity and Reversible Non-Aqueous Li-O2 Batteries. *J. Mater. Chem. A* **2013**, *1*, 13076−13081.

(27) Li, Q.; Xu, P.; Gao, W.; Ma, S.; Zhang, G.; Cao, R.; Cho, J.; Wang, H. L.; Wu, G. Graphene/Graphene-Tube Nanocomposites Templated from Cage-Containing Metal-Organic Frameworks for Oxygen Reduction in Li-O2 Batteries. *Adv. Mater.* **2014**, *26*, 1378−1386.

(28) Sun, B.; Chen, S.; Liu, H.; Wang, G. Mesoporous Carbon Nanocube Architecture for High-Performance Lithium-Oxygen Batteries. *Adv. Funct. Mater.* **2015**, *25*, 4436−4444.

(29) Wang, J.; Li, Y.; Sun, X. Challenges and Opportunities of Nanostructured Materials for Aprotic Rechargeable Lithium-Air Batteries. *Nano Energy* **2013**, *2*, 443−467.

(30) Lu, Y. C.; Gasteiger, H. A.; Shao-Horn, Y. Catalytic Activity Trends of Oxygen Reduction Reaction for Nonaqueous Li-Air Batteries. *J. Am. Chem. Soc.* **2011**, *133*, 19048−19051.

(31) Oh, S. H.; Black, R.; Pomerantseva, E.; Lee, J. H.; Nazar, L. F. Synthesis of a Metallic Mesoporous Pyrochlore as a Catalyst for Lithium-O2 Batteries. *Nat. Chem.* **2012**, *4*, 1004−1010.

(32) Black, R.; Lee, J. H.; Adams, B.; Mims, C. A.; Nazar, L. F. The Role of Catalysts and Peroxide Oxidation in Lithium-Oxygen Batteries. *Angew. Chem., Int. Ed.* **2013**, *52*, 392−396.

(33) Jian, Z.; Liu, P.; Li, F.; He, P.; Guo, X.; Chen, M.; Zhou, H. Core-Shell-Structured CNT@RuO2 Composite as a High-Performance Cathode Catalyst for Rechargeable Li-O2 Batteries. *Angew. Chem., Int. Ed.* **2014**, *53*, 442−446.

(34) Lu, J.; Lei, Y.; Lau, K. C.; Luo, X.; Du, P.; Wen, J.; Assary, R. S.; Das, U.; Miller, D. J.; Elam, J. W.; Albishri, H. M.; El-Hady, D. A.; Sun, Y. K.; Curtiss, L. A.; Amine, K. A Nanostructured Cathode Architecture for Low Charge Overpotential in Lithium-Oxygen Batteries. *Nat. Commun.* **2013**, *4*, 2383.

(35) Sun, B.; Huang, X.; Chen, S.; Munroe, P.; Wang, G. Porous Graphene Nanoarchitectures: An Efficient Catalyst for Low Charge-

DOI: 10.1021/acsami.5b07003
ACS Appl. Mater. Interfaces 2015, 7, 23182−23189

Overpotential, Long Life, and High Capacity Lithium-Oxygen Batteries. *Nano Lett.* **2014**, *14*, 3145−3152.
(36) Ottakam Thotiyl, M. M.; Freunberger, S. A.; Peng, Z.; Bruce, P. G. The Carbon Electrode in Nonaqueous Li-O2 Cells. *J. Am. Chem. Soc.* **2013**, *135*, 494−500.
(37) Itkis, D. M.; Semenenko, D. A.; Kataev, E. Y.; Belova, A. I.; Neudachina, V. S.; Sirotina, A. P.; Hävecker, M.; Teschner, D.; Knop-Gericke, A.; Dudin, P.; Barinov, A.; Goodilin, E. A.; Shao-Horn, Y.; Yashina, L. V. Reactivity of Carbon in Lithium-Oxygen Battery Positive Electrodes. *Nano Lett.* **2013**, *13*, 4697−4701.
(38) Younesi, R.; Hahlin, M.; Treskow, M.; Scheers, J.; Johansson, P.; Edström, K. Ether Based Electrolyte, LiB(CN)4 Salt and Binder Degradation in the Li-O2 Battery Studied by Hard X-ray Photoelectron Spectroscopy (HAXPES). *J. Phys. Chem. C* **2012**, *116*, 18597−18604.
(39) Nasybulin, E.; Xu, W.; Engelhard, M. H.; Nie, Z.; Li, X. S.; Zhang, J. G. Stability of Polymer Binders in Li-O2 Batteries. *J. Power Sources* **2013**, *243*, 899−907.
(40) Gittleson, F. S.; Ryu, W. H.; Taylor, A. D. Operando Observation of the Gold-Electrolyte Interface in Li-O2 Batteries. *ACS Appl. Mater. Interfaces* **2014**, *6*, 19017−19025.
(41) Zhu, D.; Zhang, L.; Song, M.; Wang, X.; Chen, Y. An In Situ Formed Pd Nanolayer as a Bifunctional Catalyst for Li-Air Batteries in Ambient or Simulated Air. *Chem. Commun.* **2013**, *49*, 9573−9575.
(42) Cui, Y.; Wen, Z.; Liu, Y. A Free-Standing-Type Design for Cathodes of Rechargeable Li-O2 Batteries. *Energy Environ. Sci.* **2011**, *4*, 4727−4734.
(43) Riaz, A.; Jung, K. N.; Chang, W.; Lee, S. B.; Lim, T. H.; Park, S. J.; Song, R. H.; Yoon, S.; Shin, K. H.; Lee, J. W. Carbon-Free Cobalt Oxide Cathodes with Tunable Nanoarchitectures for Rechargeable Lithium-Oxygen Batteries. *Chem. Commun.* **2013**, *49*, 5984−5986.
(44) Zhao, G.; Xu, Z.; Sun, K. Hierarchical Porous Co3O4 Films as Cathode Catalysts of Rechargeable Li-O2 Batteries. *J. Mater. Chem. A* **2013**, *1*, 12862−12867.
(45) Lee, H.; Kim, Y. J.; Lee, D. J.; Song, J.; Lee, Y. M.; Kim, H. T.; Park, J. K. Directly Grown Co3O4 Nanowire Arrays on Ni-Foam: Structural Effects of Carbon-Free and Binder-Free Cathodes for Lithium-Oxygen Batteries. *J. Mater. Chem. A* **2014**, *2*, 11891−11898.
(46) Hu, X.; Han, X.; Hu, Y.; Cheng, F.; Chen, J. ε-MnO2 Nanostructures Directly Grown on Ni Foam: a Cathode Catalyst for Rechargeable Li-O2 Batteries. *Nanoscale* **2014**, *6*, 3522−3525.
(47) Zhao, G.; Mo, R.; Wang, B.; Zhang, L.; Sun, K. Enhanced Cyclability of Li-O2 Batteries Based on TiO2 Supported Cathodes with No Carbon or Binder. *Chem. Mater.* **2014**, *26*, 2551−2556.
(48) Lin, X.; Shang, Y.; Huang, T.; Yu, A. Carbon-Free (Co,Mn)3O4 Nanowires@Ni Electrodes for Lithium-Oxygen Batteries. *Nanoscale* **2014**, *6*, 9043−9049.
(49) Jiang, J.; Liu, J.; Ding, R.; Ji, X.; Hu, Y.; Li, X.; Hu, A.; Wu, F.; Zhu, Z.; Huang, X. Direct Synthesis of CoO Porous Nanowire Arrays on Ti Substrate and Their Application as Lithium-Ion Battery Electrodes. *J. Phys. Chem. C* **2010**, *114*, 929−932.
(50) Zhu, L.; Wen, Z.; Mei, W.; Li, Y.; Ye, Z. Porous CoO Nanostructure Arrays Converted from Rhombic Co(OH)F and Needle-like Co(CO3)0.5(OH)·0.11H2O and Their Electrochemical Properties. *J. Phys. Chem. C* **2013**, *117*, 20465−20473.
(51) Guan, C.; Liu, J.; Cheng, C.; Li, H.; Li, X.; Zhou, W.; Zhang, H.; Fan, H. J. Hybrid Structure of Cobalt Monoxide Nanowire@Nickel Hydroxidenitrate Nanoflake Aligned on Nickel Foam for High-Rate Supercapacitor. *Energy Environ. Sci.* **2011**, *4*, 4496−4499.
(52) Yang, Z. C.; Tang, C. H.; Zhang, Y.; Gong, H.; Li, X.; Wang, J. Cobalt Monoxide-Doped Porous Graphitic Carbon Microspheres for Supercapacitor Application. *Sci. Rep.* **2013**, *3*, 2925.
(53) Liang, Y.; Wang, H.; Diao, P.; Chang, W.; Hong, G.; Li, Y.; Gong, M.; Xie, L.; Zhou, J.; Wang, J.; Regier, T. Z.; Wei, F.; Dai, H. Oxygen Reduction Electrocatalyst Based on Strongly Coupled Cobalt Oxide Nanocrystals and Carbon Nanotubes. *J. Am. Chem. Soc.* **2012**, *134*, 15849−15857.
(54) Guo, S.; Zhang, S.; Wu, L.; Sun, S. Co/CoO Nanoparticles Assembled on Graphene for Electrochemical Reduction of Oxygen. *Angew. Chem., Int. Ed.* **2012**, *51*, 11770−11773.
(55) Zhao, Y.; Sun, B.; Huang, X.; Liu, H.; Su, D.; Sun, K.; Wang, G. Porous Graphene Wrapped CoO Nanoparticles for Highly Efficient Oxygen Evolution. *J. Mater. Chem. A* **2015**, *3*, 5402−5408.
(56) Sun, B.; Liu, H.; Munroe, P.; Ahn, H.; Wang, G. Nanocomposites of CoO and a Mesoporous Carbon (CMK-3) as a High Performance Cathode Catalyst for Lithium-Oxygen Batteries. *Nano Res.* **2012**, *5*, 460−469.
(57) Dong, S.; Wang, S.; Guan, J.; Li, S.; Lan, Z.; Chen, C.; Shang, C.; Zhang, L.; Wang, X.; Gu, L.; Cui, G.; Chen, L. Insight into Enhanced Cycling Performance of Li-O2 Batteries Based on Binary CoSe2/CoO Nanocomposite Electrodes. *J. Phys. Chem. Lett.* **2014**, *5*, 615−621.
(58) Shang, C.; Dong, S.; Hu, P.; Guan, J.; Xiao, D.; Chen, X.; Zhang, L.; Gu, L.; Cui, G.; Chen, L. Compatible Interface Design of CoO-Based Li-O2 Battery Cathodes with Long-Cycling Stability. *Sci. Rep.* **2015**, *5*, 8335.
(59) Gao, R.; Liu, L.; Hu, Z.; Zhang, P.; Cao, X.; Wang, B.; Liu, X. The Role of Oxygen Vacancies in Improving the Performance of CoO as a Bifunctional Cathode Catalyst for Rechargeable Li-O2 Batteries. *J. Mater. Chem. A* **2015**, *3*, 17598−17605.
(60) Zhao, Y.; Xu, L.; Mai, L.; Han, C.; An, Q.; Xu, X.; Liu, X.; Zhang, Q. Hierarchical Mesoporous Perovskite La0.5Sr0.5CoO2.91 Nanowires with Ultrahigh Capacity for Li-Air Batteries. *Proc. Natl. Acad. Sci. U. S. A.* **2012**, *109*, 19569−19574.
(61) Zhang, Y.; Zhang, H.; Li, J.; Wang, M.; Nie, H.; Zhang, F. The Use of Mixed Carbon Materials with Improved Oxygen Transport in a Lithium-Air Battery. *J. Power Sources* **2013**, *240*, 390−396.
(62) Nasybulin, E. N.; Xu, W.; Mehdi, B. L.; Thomsen, E.; Engelhard, M. H.; Massé, R. C.; Bhattacharya, P.; Gu, M.; Bennett, W.; Nie, Z.; Wang, C.; Browning, N. D.; Zhang, J. G. Formation of Interfacial Layer and Long-Term Cyclability of Li-O2 Batteries. *ACS Appl. Mater. Interfaces* **2014**, *6*, 14141−14151.
(63) Shui, J. L.; Okasinski, J. S.; Kenesei, P.; Dobbs, H. A.; Zhao, D.; Almer, J. D.; Liu, D. J. Reversibility of Anodic Lithium in Rechargeable Lithium-Oxygen Batteries. *Nat. Commun.* **2013**, *4*, 2255.
(64) Adams, B. D.; Radtke, C.; Black, R.; Trudeau, M. L.; Zaghib, K.; Nazar, L. F. Current Density Dependence of Peroxide Formation in the Li-O2 Battery and Its Effect on Charge. *Energy Environ. Sci.* **2013**, *6*, 1772−1778.
(65) Rinaldi, A.; Wijaya, O.; Hoster, H. E.; Yu, D. Y. W. History Effects in Lithium-Oxygen Batteries: How Initial Seeding Influences the Discharge Capacity. *ChemSusChem* **2014**, *7*, 1283−1288.
(66) Su, D.; Dou, S.; Wang, G. Gold Nanocrystals with Variable Index Facets as Highly Effective Cathode Catalysts for Lithium-Oxygen Batteries. *NPG Asia Mater.* **2015**, *7*, e155.
(67) Gallant, B. M.; Kwabi, D. G.; Mitchell, R. R.; Zhou, J.; Thompson, C. V.; Shao-Horn, Y. Influence of Li2O2Morphology on Oxygen Reduction and Evolution Kinetics in Li-O2 Batteries. *Energy Environ. Sci.* **2013**, *6*, 2518−2528.
(68) Hu, Y.; Han, X.; Cheng, F.; Zhao, Q.; Hu, Z.; Chen, J. Size Effect of Lithium Peroxide on Charging Performance of Li-O2 Batteries. *Nanoscale* **2014**, *6*, 177−180.
(69) McCloskey, B. D.; Scheffler, R.; Speidel, A.; Girishkumar, G.; Luntz, A. C. On the Mechanism of Nonaqueous Li-O2 Electrochemistry on C and Its Kinetic Overpotentials: Some Implications for Li-Air Batteries. *J. Phys. Chem. C* **2012**, *116*, 23897−23905.

DOI: 10.1021/acsami.5b07003
ACS Appl. Mater. Interfaces 2015, 7, 23182−23189